Kinesthetic teaching of bi-manual tasks with known relative constraints

Sotiris Stavridis, Dimitrios Papageorgiou and Zoe Doulgeri

Abstract— **Kinesthetic teaching allows the direct skill transfer from the human to the robot and has been widely used to teach single arm tasks intuitively. In the bi-manual case, simultaneously moving both end-effectors is challenging due to the high physical and cognitive load imposed to the user. Thus, previous works on bi-manual task teaching resort to less intuitive methods by teaching each arm separately. This in turn requires motion synthesis and synchronization before execution. In this work, we leverage knowledge from the relative task space to facilitate a kinesthetic demonstration by guiding both end-effectors which is more human-like and intuitive way for performing bi-manual tasks. Our method utilizes the notion of virtual fixtures and inertia minimization in the null space of the task. The controller is experimentally validated in a bi-manual task which involves the drawing of a preset line on a workpiece utilizing two KUKA IIWA7 R800 robots. Results from ten participants were compared with a gravity compensation scheme demonstrating improved performance.**

I. Introduction

Kinesthetic teaching is commonly utilized in literature for tackling the problem of Learning by Demonstration (LbD). It allows the human-teacher to physically interact with the robot for demonstrating a desired kinematic behavior. The main advantages of kinesthetic teaching come from its direct nature, as the motion is demonstrated directly on the robot by the human-teacher who physically interacts with it [1]. In this way, no mapping of the motion is required for transferring the kinematic skills, as opposed to other LbD methods, such as when the human demonstrates the task with its motion being captured by video and/or other external sensors, also known as the correspondance problem [1], [2].

Kinesthetic teaching has been widely used for teaching end-effector skills to single robotic manipulators [3]–[7]. However, in many tasks, a bi-manual solution is required which allows a bigger workspace and an enhanced dexterity/maneuverability owing to the redundant DOFs. To the best of our knowledge there are no works that demonstrate a bi-manual task in the relative space by simultaneously guiding both arms. In [8] a bi-manual peg-in-hole is demonstrated by manually guiding one arm in the relative space, while the other remains static which may be impractical due to the kinematic limits of the single robot structure. In [9], [10], demonstration of the motion of each end-effector is performed separately. In the reproduction phase, the demonstrated motion segments have to be smoothly sequenced and synchronized to reproduce the overall demonstrated motions. In all the above works the kinesthetic demonstration of a bi-manual task does not involve the simultaneous guiding of the two arms unless the relative pose is fixed as when showing the transferring of a box rigidly grasped by the two arms [10]. Demonstrating the relative motion between end-effectors is a more cognitively and physically demanding task than its single arm counterpart, arising from the fact that the human-teacher has to utilize both their hands simultaneously facing high cognitive and physical load [11], particularly when the task involves the contact between two parts.

Task knowledge has been used to assist the human-teacher in demonstrating a single arm task involving contact via virtual fixtures (VF) placed appropriately in the task space [6], [7], [12]–[16]. Moreover, inertia minimization has been utilized in redundant manipulators to reduce the effective end-effector inertia during kinesthetic guidance [17]–[19].

In this work, we utilize VF based on the knowledge of the workpiece's geometry, inertia optimization and joint limit avoidance to assist teaching of a bi-manual task involving contact with the workpiece's surface by simultaneously guiding the two end-effectors. To the best of our knowledge this is the first time a shared controller that achieves all these objectives is proposed, theoretically justifying its passivity as well as the satisfaction of the joint limits. We further demonstrate how we can successfully teach such a task maintaining contact with reduced teaching duration and physical load.

II. Problem formulation and Concept solution

Let us consider the kinesthetic teaching of a bi-manual task to a robot possessing two manipulators. In order for the human to kinesthetically demonstrate the motion to the robot, the parts involved in the task e.g. a workpiece and a tool, are already firmly grasped by the robot's manipulators and the human has to grab the robot's end-effectors with both their hands and physically guide the robot. If the arms are only under gravity compensation, the human has to account for the task constraints and joint limits while being affected by disturbances mainly from the unmodelled robot dynamics. We address the problem of controlling the bi-manual robot in such a way so that the user is facilitated in their task by reducing their cognitive and physical load.

In many applications, knowledge of Relative Task Constrains (RTC) is available as they can be defined by the CAD models of the parts involved in the task. Such constraints, for example, can be defined for a process that is performed at the upper surface of a workpiece with known CAD model, where a tool must be in orthogonal contact with the surface. Rather than planning a trajectory in a complex space, i.e.

The research leading to these results has received funding from the European Community's Framework Programme Horizon 2020 under grant agreement No 871704, project BACCHUS

Authors are with the Dept. of Electrical and Computer Engineering, Aristotle University of Thessaloniki, Greece.
sotistav@ece.auth.gr,dimpapag@ece.auth.gr, doulgeri@ece.auth.gr

on the surfaces of curved objects, which is a difficult and time-consuming task, a trajectory may be demonstrated by a user and encoded in a DMP from a single demonstration allowing spatial generalization, for example in size variants of the workpiece.

Given the availability of such a knowledge, we propose the utilization of two VF signals for reducing the human's cognitive load, so that they do not have to consciously account for the satisfaction of the task and joint constraints. They are based on two different artificial potentials: a) a task VF for facilitating the user and b) barrier VF in the joint space to ensure the evolution of the robot's joint positions within their limits. The task VF facilitates establishing and maintaining contact between the workpiece and the tool, within the limits of the former, by a high stiffness attractive potential.

Furthermore, the reduction of the physical load of the human is addressed by the on-line minimization of the inertial forces between the human and the robot along the allowable directions of motion with respect to the task. This optimization signal exploits the redundant DOFs of the bi-manual robot, as it is projected into its relative dynamic null space in order to not affect the relative task.

A. Kinematics and dynamics of the shared control system

Consider a bi-manual robot setup with each robot having n-DOFs and $\mathbf{q} = [\mathbf{q}_1^\intercal \ \mathbf{q}_2^\intercal]^\intercal \in \mathbb{R}^{2n}$ being its joint variables. Let $\mathbf{x}_i(\mathbf{q}) \triangleq [\mathbf{p}_i(\mathbf{q})^\intercal \ \mathbf{Q}_i(\mathbf{q})^\intercal]^\intercal \in \mathcal{T}$, for $i = \{1, 2\}$, be the end-effector pose of the first and second manipulator respectively, where $\mathcal{T} \triangleq \mathbb{R}^3 \times \mathbb{S}^3 \equiv SE(3)$, with $\mathbf{p}_i \in \mathbb{R}^3$ being the position and $\mathbf{Q}_i = [\eta_i \ \boldsymbol{\epsilon}_i^\intercal]^\intercal \in \mathbb{S}^3$ being the orientation represented by a unit quaternion, while $\eta_i \in [-1, 1]$ is the scalar and $\boldsymbol{\epsilon}_i \in \mathbb{R}^3$ the vector part of the quaternion. The joint space equations of motion of the $2n$-DOFs bi-manual robot with gravity compensation and shared control is described by:

$$\begin{bmatrix} \mathbf{H}_1 & \mathbf{0} \\ \mathbf{0} & \mathbf{H}_2 \end{bmatrix} \begin{bmatrix} \ddot{\mathbf{q}}_1 \\ \ddot{\mathbf{q}}_2 \end{bmatrix} + \begin{bmatrix} \mathbf{C}_1 & \mathbf{0} \\ \mathbf{0} & \mathbf{C}_2 \end{bmatrix} \begin{bmatrix} \dot{\mathbf{q}}_1 \\ \dot{\mathbf{q}}_2 \end{bmatrix} = \begin{bmatrix} \mathbf{J}_1 & \mathbf{0} \\ \mathbf{0} & \mathbf{J}_2 \end{bmatrix}^\intercal \begin{bmatrix} \mathbf{F}_1 \\ \mathbf{F}_2 \end{bmatrix} + \begin{bmatrix} \mathbf{u}_1 \\ \mathbf{u}_2 \end{bmatrix}, \quad (1)$$

where $\mathbf{q}_i \in \mathbb{R}^n$ with $i = \{1, 2\}$ is the vector of joint positions, $\mathbf{J}_i(\mathbf{q}_i) \in \mathbb{R}^{6\times n}$ is the robot Jacobian, $\mathbf{H}_i(\mathbf{q}_i) \in \mathbb{R}^{n\times n}$ is the positive definite inertia matrix, $\mathbf{C}_i(\mathbf{q}_i, \dot{\mathbf{q}}_i) \in \mathbb{R}^{n\times n}$ is the Coriolis and centripetal matrix, with $\dot{\mathbf{H}}_i - 2\mathbf{C}_i$ being skew symmetric, $\mathbf{F}_i \in \mathbb{R}^6$ is the human generalized force applied to the i-th end-effector during the kinesthetic teaching and $\mathbf{u}_i \in \mathbb{R}^n$ is the control signal to be designed in order to facilitate the human in teaching the task. Let $\mathbf{u} = [\mathbf{u}_1^\intercal \ \mathbf{u}_2^\intercal]^\intercal \in \mathbb{R}^{2n}$ be synthesized by a task space signal, a joint space signal and a dynamic null space signal, which are combined as follows:

$$\mathbf{u} = \mathbf{J}_R^\intercal(\mathbf{q})\mathbf{u}_R + \mathbf{u}_J + \mathbf{u}_N, \quad (2)$$

where $\mathbf{u}_R \in \mathbb{R}^6$ is the relative task space control signal that renders the VF for RTC enforcement, $\mathbf{u}_J \in \mathbb{R}^{2n}$ is a control signal that renders the VF for joint limit avoidance, $\mathbf{u}_N \in \mathbb{R}^{2n}$ is a control signal for the minimization of the inertial forces experienced by the user, and $\mathbf{J}_R \in \mathbb{R}^{6\times 2n}$ is the relative task space Jacobian of the two end-effectors which is given by:

$$\mathbf{J}_R \triangleq \begin{bmatrix} \mathbf{R}_2^\intercal & \mathbf{0} \\ \mathbf{0} & \mathbf{R}_2^\intercal \end{bmatrix} \begin{bmatrix} \mathbf{I}_6 & -\begin{bmatrix} \mathbf{I}_3 & -\mathbf{S}(\mathbf{p}_{21}) \\ \mathbf{0} & \mathbf{I}_3 \end{bmatrix} \end{bmatrix} \begin{bmatrix} \mathbf{J}_1 & \mathbf{0} \\ \mathbf{0} & \mathbf{J}_2 \end{bmatrix} \quad (3)$$

and is expressed with respect to the second end-effector that holds the workpiece with $\mathbf{R}_2 \in SO(3)$ being the rotation matrix of the orientation of the second end-effector and $\mathbf{S}(\mathbf{p}_{21})$ the skew-symmetric matrix of the displacement vector between the two end-effectors $\mathbf{p}_{21} = -\mathbf{p}_2 + \mathbf{p}_1$.

Let $\mathbf{x}_R(\mathbf{q}) \triangleq [\mathbf{p}_R(\mathbf{q})^\intercal \ \mathbf{Q}_R(\mathbf{q})^\intercal]^\intercal \in \mathcal{T}$ be the relative pose between the two end-effectors, where $\mathbf{p}_R = \mathbf{R}_2^\intercal(\mathbf{p}_1 - \mathbf{p}_2) \in \mathbb{R}^3$ is the relative translation, $\mathbf{Q}_R = \overline{\mathbf{Q}}_2\mathbf{Q}_1 = [\eta \ \boldsymbol{\epsilon}^\intercal]^\intercal \in \mathbb{S}^3$ the unit quaternion of the relative orientation $\overline{\mathbf{Q}}_2$ denoting the quaternion conjugate of $\mathbf{Q}_2$. The mapping from the relative velocity of the end-effectors $\mathbf{v}_R \triangleq [\dot{\mathbf{p}}_R^\intercal \ \boldsymbol{\omega}_R^\intercal]^\intercal \in \mathbb{R}^6$, with $\dot{\mathbf{p}}_R, \boldsymbol{\omega}_R \in \mathbb{R}^3$ being the relative linear and angular velocity respectively, to $\dot{\mathbf{x}}_R$ is

$$\dot{\mathbf{x}}_R = \mathbf{J}_v(\mathbf{x}_R)\mathbf{v}_R, \quad (4)$$

with $\mathbf{J}_v(\mathbf{x}) \triangleq \operatorname{diag}\left(\mathbf{I}_3, \frac{1}{2}\mathbf{J}_Q(\mathbf{Q})\right)$ and $\mathbf{J}_Q(\mathbf{Q}) \triangleq \begin{bmatrix} -\boldsymbol{\epsilon} & \eta\mathbf{I}_3 + \mathbf{S}(\boldsymbol{\epsilon}) \end{bmatrix}^\intercal \in \mathbb{R}^{4\times 3}$.

B. Relative Task Constraint

Let $\mathbf{x}_c(\boldsymbol{\sigma})$ denote a parametric expression of the valid poses of the 1st manipulator, i.e. $\mathbf{x}_1$, with respect to the frame of the end-effector of the 2nd manipulator according to the RTC:

$$\mathbf{x}_c(\boldsymbol{\sigma}) \triangleq \begin{bmatrix} \mathbf{p}_c(\boldsymbol{\sigma}) \\ \mathbf{Q}_c(\boldsymbol{\sigma}) \end{bmatrix} : \mathbb{R}^m \to \mathcal{T}, \quad (5)$$

where $\boldsymbol{\sigma} \in \mathbb{R}^m$ is the vector of minimum required parameters to describe the RTC and $m \leq 6$ the RTC DOFs. Such constraints in the form of parametric expressions can be easily extracted by the CAD model of the parts; for instance for $m = 1$ the motion is constrained on a curve which can be defined by a B-spline and for $m = 2$ the motion is constrained on a surface which can be defined by Non-uniform Rational B-splines (NURBS), which are commonly used expressions in CAD design. Examples of such parametric expressions can be found in [12].

The allowable directions of motion, are determined by the columns of the following matrix, which involves both translation and orientation:

$$\mathbf{J}_c(\boldsymbol{\sigma}) \triangleq \begin{bmatrix} \mathbf{I}_3 & \mathbf{0} \\ \mathbf{0} & 2\mathbf{J}_Q(\mathbf{Q}_c(\boldsymbol{\sigma}))^\intercal \end{bmatrix} \frac{\partial \mathbf{x}_c(\boldsymbol{\sigma})}{\partial \boldsymbol{\sigma}} \in \mathbb{R}^{6\times m}. \quad (6)$$

Notice that by formulating the task geometry with respect to the moving end-effector frame that holds the workpiece, the RTC remains static in the relative space.

III. Proposed controller

A. Virtual fixture for RTC

To assist the human-teacher by communicating the directions towards the satisfaction of the RTC, we propose the utilization of penetrable VF initially proposed in [7] for a single robot. In the bi-manual kinesthetic teaching task,

the VF are not fixed with respect to the inertial frame but are utilized in the relative space and the control action is distributed in both robotic manipulators using the relative Jacobian (2), (3). In particular, the VF are enforced by the control action (i.e., $\mathbf{u}_R$) which generates attractive forces for both end-effectors towards the nearest relative pose that belongs to the set $\mathbf{x}_c$.

Let the actual relative pose be $\mathbf{x}_R$, which can be calculated from the pose of each end-effector $\mathbf{x}_1$ and $\mathbf{x}_2$. For calculating the control action, the closest pose in the RTC set from $\mathbf{x}_R$ has to be found at every control cycle. To achieve this, one has to solve online the following optimization problem and then calculate $\mathbf{x}_c(\boldsymbol{\sigma}^*)$:

$$\boldsymbol{\sigma}^* = \underset{\boldsymbol{\sigma}\in\Omega_\sigma}{\arg\min}\, \phi(\mathbf{x}_R, \mathbf{x}_c(\boldsymbol{\sigma})) \tag{7}$$

where

$$\phi(\mathbf{x}_R, \mathbf{x}_c) \triangleq \frac{\|\mathbf{e}_p\|^2}{\overline{r}^2} + \frac{\|\mathbf{e}_o\|^2}{\overline{s}^2}, \tag{8}$$

is a generalized metric between the two poses $\mathbf{x}_R = [\mathbf{p}_R^\intercal \;\; \mathbf{Q}_R^\intercal]^\intercal$ and $\mathbf{x}_c = [\mathbf{p}_c^\intercal \;\; \mathbf{Q}_c^\intercal]^\intercal$ with $\mathbf{e}_p \triangleq \mathbf{p}_R - \mathbf{p}_c$ and $\mathbf{e}_o \triangleq \mathrm{Im}(\overline{\mathbf{Q}}_c\mathbf{Q}_R)$ is the vector part of the quaternion difference, $\overline{r}, \overline{s} \in \mathbb{R}^+$ constant positive weights, $\|.\|$ denotes the Euclidean norm while Ω_σ denotes the rectangular region of the parametric space. Notice that by selecting $\overline{s} = \sin\frac{\overline{\theta}}{2}$ with $\overline{\theta}$ being a positive parameter, $\phi < 1$ if and only if $\|\mathbf{p}_R - \mathbf{p}_c\| < \overline{r}$ and the angle between the two frames is less than $\overline{\theta}$. Assuming the local convexity of (7) and given the smoothness of $\mathbf{x}_c(\boldsymbol{\sigma})$ by construction, (7) can be solved on-line by the gradient descent law:

$$\dot{\boldsymbol{\sigma}}^* \triangleq -k_g \left.\frac{\partial\phi(\mathbf{x}_R, \mathbf{x}_c(\boldsymbol{\sigma}))}{\partial\boldsymbol{\sigma}}\right|_{\boldsymbol{\sigma}=\boldsymbol{\sigma}^*}. \tag{9}$$

The task VF is built upon the notion of artificial potentials. This means that the control action is computed by the gradient of a scalar potential function of the relative pose. In particular, the control action is calculated by:

$$\mathbf{u}_R = -\mathbf{J}_v^\intercal(\mathbf{x}_R)\frac{\partial U(\mathbf{x}_R, \mathbf{x}_c(\boldsymbol{\sigma}^*))}{\partial\mathbf{x}_R} - \mathbf{D}\mathbf{v}_R, \tag{10}$$

with $\mathbf{D} \in \mathbb{R}^{6\times6}$ being a positive definite damping matrix introducing the active damping and $U(\mathbf{x}_R, \mathbf{x}_c(\boldsymbol{\sigma})) : \mathcal{T}\times\mathcal{T} \to \mathbb{R}^+$ being the potential function. The following potential function similar to [7] is utilized:

$$U(\mathbf{x}, \mathbf{x}_c(\boldsymbol{\sigma})) \triangleq k_p f\left(\frac{\|\mathbf{e}_p\|}{\overline{r}}\right) + k_o f\left(\frac{\|\mathbf{e}_o\|}{\overline{s}}\right), \tag{11}$$

where $k_p, k_o \in \mathbb{R}_{>0}$ are tunable gains and $f(x) : \mathbb{R}_{\geq0} \to \mathbb{R}_{\geq0}$ is the following C^1-smooth function shown in Fig.1a:

$$f(y) \triangleq \begin{cases} (3-g)y^2 + (g-2)y^3, & \text{if } y < 1 \\ g(y-1) + 1, & \text{if } y \geq 1 \end{cases}, \tag{12}$$

with $g \in (0, 3]$. Its derivative $\frac{\partial f(y)}{\partial y}$ is proportional to the force and torque magnitude transmitted to the user. Notice that the specific selection of U distinguishes the relative task space in two regions, the "high stiffness" and the free space region based on the distance from the RTC set. The parameters $\overline{r}$ and $\overline{s}$ define the boundary between those two regions for translation and orientation respectively. In free space for $y > 1$, $\frac{\partial f(y)}{\partial y}$ is constant and equal to g, which corresponds to a relatively small constant force magnitude so that the user is able to freely move the end-effectors at the beginning and the end of the kinesthetic teaching while being aware of the direction in which the RTC set lies. In the high stiffness area the forces transferred to the user facilitate the user in satisfying the RTC constraints.

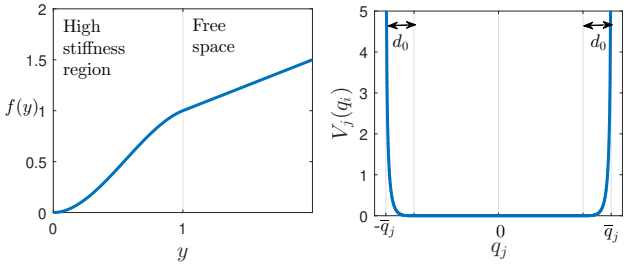

(a) VF for RTC. **(b)** VF for joint limit avoidance.

Fig. 1: Artificial potentials utilized for the VF signals.

B. Virtual fixtures for joint limit avoidance

Joints limits are also constraints that the user should be aware of when manually guiding the robot. We propose the utilization of VF in the whole joint space. These VF together with the task VF may introduce local minima in the relative space. However, such a problem did not occur in our experimental evaluation. This may be attributed to the robot's high redundancy with respect to the relative task DOFs.

Assuming symmetrical joint limits, the control signal $\mathbf{u}_J$ for each joint $(j = 1, 2, ..., 2n)$ is given by:

$$u_j = -k_{dq}\dot{q}_j - \begin{cases} k_q\frac{\mathrm{sign}(q_j)(\overline{q}_j - |q_j| - d_0)}{\psi_j d_0^2}\ln(\psi_j), & \text{if } |q_j| > \overline{q}_j - d_0 \\ 0, & \text{if } |q_j| \leq \overline{q}_j - d_0 \end{cases}, \tag{13}$$

where

$$\psi_j(q_j) \triangleq 1 - \frac{(\overline{q}_j - |q_j| - d_0)^2}{d_0^2} \tag{14}$$

with k_q, k_{dq} being positive gains, d_0 defining the activation distance from the joint limit respectively and q_j and $\overline{q}_j$ the current joint position and joint limit absolute values respectively. The sign of the second term of (13) becomes negative when approaching the upper joint limits and positive when approaching the lower joint limits. This signal (13) is derived from the artificial potential function shown in Fig.1b and which is given by:

$$V_J(\mathbf{q}) \triangleq k_q \sum_{j=1}^{2n} \frac{1}{4}\ln^2\left(\psi_j(q_j)\right). \tag{15}$$

This is a positive continuously differentiable scalar function for all $(\overline{q}_j - |q_j|) \in \mathbb{R}^+$, V and $\|\frac{\partial V}{\partial q_j}\|$ approaches ∞ if and only if $(\overline{q}_j - |q_j|) \to 0$, V and $\|\frac{\partial V}{\partial q_j}\|$ is zero if and only if $\overline{q}_j - |q_j| > d_0$, and consequently $u_j = 0$.

C. Passivity proof of VF control and satisfaction of the joint limit constraints

Let $\mathbf{v} = [\mathbf{v}_1^\intercal \ \mathbf{v}_2^\intercal]^\intercal \in \mathbb{R}^{12}$ be the vector of generalized velocities of the two end-effectors $\mathbf{v}_i \in \mathbb{R}^6$, $i = 1, 2$ and $\mathbf{F}_h = [\mathbf{F}_1^\intercal \ \mathbf{F}_2^\intercal]^\intercal \in \mathbb{R}^{12}$ be the vector of generalized external forces applied to each end-effector $\mathbf{F}_i \in \mathbb{R}^6$, $i = 1, 2$.

Theorem 1: For the closed loop system (1), (2), (10) and (13), with $\mathbf{u}_N = \mathbf{0}$, the following statements are true:

1) The system is strictly output passive with respect to the end-effectors velocities $\mathbf{v}$, under the exertion of the interaction force $\mathbf{F}_h$.
2) The evolution of the joint positions will always belong to the hyper-rectangle defined by the joint limits, i.e., $\mathbf{q}(t) \in \Omega, \forall t$, where $\Omega \triangleq \{\mathbf{q} \in \mathbb{R}^{2n} : |q_i| < \overline{q}_i, \forall i = 1, 2, ..., 2n\}$, given any $\mathbf{q}(t_0) \in \Omega$, under the exertion of a bounded interaction force $\mathbf{F}_h$ applied by the human.

Proof: For the closed loop system, consider the following storage function:

$$V \triangleq \frac{1}{2}\dot{\mathbf{q}}^\intercal \mathbf{H} \dot{\mathbf{q}} + U(\mathbf{x}, \mathbf{x}_c(\boldsymbol{\sigma}^*)) + V_J(\mathbf{q}), \tag{16}$$

where $\mathbf{H} = \text{diag}(\mathbf{H}_1, \mathbf{H}_2)$. Notice that $V_J(\mathbf{q}) = +\infty$ if and only if $\mathbf{q} \in \partial\Omega$. Utilizing (9), the time derivative of the potential function $U(\mathbf{x}, \mathbf{x}_c(\boldsymbol{\sigma}^*))$ is:

$$\dot{U}(\mathbf{x}, \mathbf{x}_c^*) = \dot{\mathbf{x}}^\intercal \tfrac{\partial U(\mathbf{x}, \mathbf{x}_c^*)}{\partial \mathbf{x}} - k_g \left(\tfrac{\partial \phi}{\partial \boldsymbol{\sigma}}\Big|_{\boldsymbol{\sigma}=\boldsymbol{\sigma}^*} \right)^\intercal \tfrac{\partial U(\mathbf{x}, \mathbf{x}_c^*)}{\partial \boldsymbol{\sigma}^*} \tag{17}$$

with $\mathbf{x}_c^* = \mathbf{x}_c(\boldsymbol{\sigma}^*)$. Assuming that the nearest pose is found within a control cycle, the second term of (17) is 0, as $\tfrac{\partial \phi}{\partial \boldsymbol{\sigma}}\Big|_{\boldsymbol{\sigma}=\boldsymbol{\sigma}^*} = 0$ at each control cycle. Thus, the following result holds for the time derivative of (16) by taking into account $\dot{\mathbf{x}}_R = \mathbf{J}_v \mathbf{v}_R$ and $\mathbf{v} = \mathbf{J}\dot{\mathbf{q}}$:

$$\dot{V} = \mathbf{v}^\intercal \mathbf{F}_h - \dot{\mathbf{q}}^\intercal \left(k_{dq}\mathbf{I} + \mathbf{J}_R^\intercal \mathbf{D} \mathbf{J}_R\right) \dot{\mathbf{q}} \tag{18}$$

with $k_{dq}\mathbf{I} + \mathbf{J}_R^\intercal \mathbf{D} \mathbf{J}_R$ being positive definite and thus the system is strictly output passive. By completing the squares, (18) becomes:

$$\begin{aligned} \dot{V} &\leq \dot{\mathbf{q}}^\intercal \mathbf{J}^\intercal \mathbf{F}_h - \lambda_D \dot{\mathbf{q}}^\intercal \dot{\mathbf{q}} \\ &\leq -\|\sqrt{\lambda_D}\dot{\mathbf{q}} - \frac{1}{2\sqrt{\lambda_D}} \mathbf{J}^\intercal \mathbf{F}_h\|^2 + \frac{1}{4\lambda_D}\|\mathbf{J}^\intercal \mathbf{F}_h\|^2 \\ &\leq \frac{1}{4\lambda_D}\|\mathbf{J}^\intercal \mathbf{F}_h\|^2, \end{aligned} \tag{19}$$

with $\lambda_D \triangleq \lambda_{min}(k_{dq}\mathbf{I} + \mathbf{J}_R^\intercal \mathbf{D} \mathbf{J}_R) \in \mathbb{R}_{>0}$ denoting the minimum eigenvalue, while $\mathbf{J} = \text{diag}(\mathbf{J}_1, \mathbf{J}_2)$. Integrating (19), we get:

$$V(t) \leq V(t_0) + \int_{t_0}^{t} \frac{1}{4\lambda_D}\|\mathbf{J}^\intercal \mathbf{F}_h\|^2 dt, \forall t > t_0, \tag{20}$$

which means that $V(t)$ will be bounded, given that the force applied by the human is of bounded energy. Thus, due to (16), the joint positions will never reach their limits, when starting within Ω. ■

D. Null space inertia minimization

To reduce the physical load that the user experiences during manual guidance we propose the reduction of the interaction forces by means of minimizing the effective inertia of the manipulator along the directions of motion defined by the RTC. The cost function to be minimized consists of the weighted sum of two metrics, namely $c_t(\mathbf{q}) \in \mathbb{R}^+$ and $c_\omega(\mathbf{q}) \in \mathbb{R}^+$, which are related to the effective inertia in the relative task space along the directions of the RTC in translation and orientation respectively. In particular, the cost function is defined as:

$$c(\mathbf{q}) \triangleq \kappa c_v(\mathbf{q}) + \lambda c_\omega(\mathbf{q}), \tag{21}$$

where $\kappa, \lambda \in \mathbb{R}^+$ the constant weights for translation and orientation respectively. The metrics $c_v(\mathbf{q}), c_\omega(\mathbf{q})$ are determined based on the pseudo-kinetic energy matrices [20] of the manipulator and are given by:

$$c_i \triangleq \det\left(\mathbf{T}_i(\mathbf{x}_c(\boldsymbol{\sigma}^*))^\intercal \boldsymbol{\Lambda}_{R,i}^{-1}(\mathbf{q}) \mathbf{T}_i(\mathbf{x}_c(\boldsymbol{\sigma}^*))\right)^{-1}, \tag{22}$$

where $i = \{v, \omega\}$ and $\mathbf{T}_i \in \mathbb{R}^{3 \times m_i}$ a matrix whose columns form an orthonormal basis which spans the column space of the translational ($i = v$) and rotational ($i = \omega$) part of $\mathbf{J}_c$, with m_i being the DOFs involved in translation and orientation part of the RTC separately, while $\boldsymbol{\Lambda}_{R,i} = (\mathbf{J}_{R,i}\mathbf{H}^{-1}\mathbf{J}_{R,i}^\intercal)^{-1}$ are the respective relative space pseudo-kinetic energy matrices. The metric (22) describes the effective mass/inertia towards the unconstrained directions of the task. Taking the negative gradient of the inertia metric (21) in the configuration space, i.e. $-\frac{\partial c}{\partial \mathbf{q}}$, and performing gradient descent, a local minimum of the effective inertia metric can be reached. In order to minimize (21) without affecting the task, the redundancy of the manipulator is exploited by projecting the gradient of (21) into the dynamic relative null space using the dynamic relative null space projection matrix given by: $\mathbf{N}_R = \mathbf{I} - \bar{\mathbf{J}}_R \mathbf{J}_R$, with $\bar{\mathbf{J}}_R = \mathbf{H}^{-1}\mathbf{J}_R^\intercal(\mathbf{J}_R\mathbf{H}^{-1}\mathbf{J}_R^\intercal)^{-1}$ being the dynamic relative Jacobian pseudoinverse. Projecting the optimization signal into the relative null space, instead of the individual end-effector null space, induces generalized forces in the absolute space that guide the user to an improved pose with respect to the task.

Moreover, to avoid high values of the metric gradient along the joint space domain, a smooth saturation function of the form $\mathbf{f}_{sat}(\mathbf{y}) \triangleq \overline{\tau}\tanh\left(\frac{\|\mathbf{y}\|}{\overline{\tau}}\right)\frac{\mathbf{y}}{\|\mathbf{y}\|}$ is used to limit the optimization signal to safe levels, where $\overline{\tau} \in \mathbb{R}^+$ is the bound of the torque norm for a given $\mathbf{y} \in \mathbb{R}^n$. The null space projected torque is then given by:

$$\mathbf{u}_N = \mathbf{N}_R^\intercal \left(-\mathbf{f}_{sat}\left(k_c \frac{\partial c}{\partial \mathbf{q}}\right) - k_d \mathbf{H}\dot{\mathbf{q}}\right), \tag{23}$$

where the damping term $-k_d\mathbf{H}\dot{\mathbf{q}}$ ensures that $-k_d\dot{\mathbf{q}}^\intercal \mathbf{N}_R^\intercal \mathbf{H}\dot{\mathbf{q}} \leq 0$ and thus it is dissipative [21].

Remark 1: To ensure passivity of the closed loop system, consisted of (1), (2), (10), (13) and (23), one could utilize the notion of energy tanks similarly to [7]. In this case, a portion of the dissipated energy of the closed loop system could have been considered to be stored in an energy tank, which in turn

would allow the inertia optimization to be performed when it is not depleted.

IV. Experimental results

To validate and evaluate the performance of the proposed controller, drawing over a marked path on a curved workpiece with a marker, as seen in Fig.2b, is considered. This task has similarities with common industrial tasks, such as welding, milling, finishing, etc. Two KUKA IIWA7 R800 robots have been utilized for this experiment. The workpiece is attached to the left arm while the marker to the right arm as seen in Fig.2. In order to properly draw a line on the workpiece, the user has to maintain orthogonal contact with the surface of the workpiece. Three parameters are

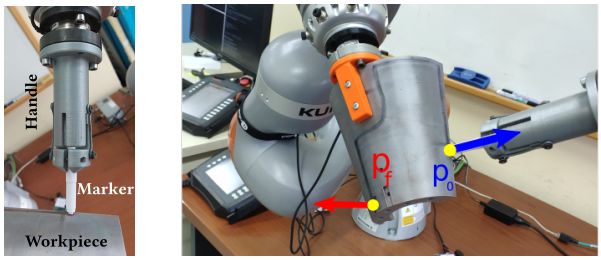

(a) Marker tool **(b)** The considered drawing task.

Fig. 2: Experiment. The users were asked to kinesthetically guide the marker tool to draw from p_0 (blue) to p_f (red) over the black line on the workpiece. Arrows denote the normal vectors.

sufficient to describe the RTC. The parametric expression describing the external surface of the workpiece is given by: $\mathbf{p}_c(\sigma_1, \sigma_2) = [r(\sigma_1)\cos(\pi - \sigma_2) \quad \sigma_1 \quad r(\sigma_1)\sin(\pi - \sigma_2)]^\intercal$, where $r(\sigma_1) = 0.075 - \sigma_1 \tan(\pi/18)$, and the following for orientation $\mathbf{R}_c(\sigma_2, \sigma_3) = \mathbf{R}_y(\pi/2 + s_2)\mathbf{R}_x(\pi/18)\mathbf{R}_z(\sigma_3)$ in rotation matrix form. The physical interpretation of $\sigma_1, \sigma_2, \sigma_3$ can be seen in Fig.3. The bounds in translation

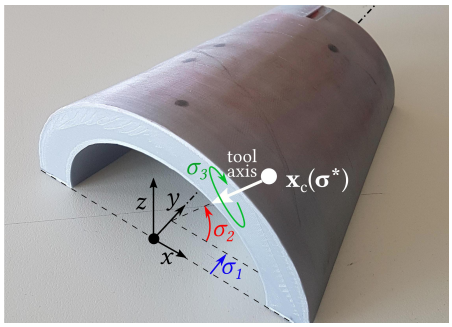

Fig. 3: The object utilized for the experiment, with its upper surface representing the spatial constraint.

and orientation for the VF, i.e., for (11), are selected to be $\bar{r} = 0.02$m and $\bar{\theta} = 0.174$rad respectively. The control parameters are set to $k_p = k_o = 0.5$, $\mathbf{D} = 0.5\mathbf{I}_6$, $g = 0.1$ for (12). The joint limit avoidance control parameters are set to $k_{dq} = 0.001, k_q = 0.15$ and $d_0 = 0.0698rad$. The joint limits are $\bar{q} = [170\ 120\ 170\ 120\ 170\ 120\ 175]^o$ for each arm. For the null space inertia optimization the parameter values are: $\kappa = 20, \lambda = 300$ for (21) and $k_c = 2.0, k_d = 0.01$ for (23), while the commanded signal norm is saturated at $\bar{\tau} = 4$Nm. The control cycle is 2ms.

We compare the proposed framework with a gravity compensation controller (GC) with the damping elements of the proposed controller for a fair comparison i.e. $k_c = k_p = k_o = 0$ in (11) and (23). The joint limit avoidance signal (13) is also enabled in GC. Furthermore, an audio feedback is played to warn the user that the angle of the marker tool and the normal to the RTC is outside the desired region, i.e. $\|e_o\| > 0.087$rad, and the line is not properly drawn. Ten participants have been asked to do a single demonstration of the task, i.e. drawing on the marked path seen in Fig.2b, using the proposed methodology and the gravity compensation controller. Two ATI mini40 F/T sensors mounted on the wrists of the manipulators have been used to measure the forces exerted by the users at the end-effectors. Before the demonstration, the users did one test run with the proposed and the GC methods in order to familiarize themselves with the task. The initial robot configuration was the same for all users, but variability between users resulted in different robot configurations at the time of initial contact of the tool with the workpiece. The total demonstration time, the energy exchanged between the human and the robot (E), the energy transmitted from the user to the robot (E^+), the mean distance of the marker tool from the RTC ($\mu(||e_p||)$) and the mean angle between the marker tool and the normal to the RTC vector ($\mu(||e_o||)$) were considered as evaluation criteria, since they reflect the physical and cognitive load, and how well the user executes the task, i.e. respects the constraints. The measurements were logged from the moment the marker makes contact with the workpiece until it reaches the end of the marked path, i.e. p_0 and p_f in Fig.2b, respectively. Notice in Fig.2a the head of the marker is flat, consequently even a slight error in position or orientation would result in contact loss and a partially drawn line. Fig.4 shows a boxplot of the percentage change between the metrics of GC and the proposed method, e.g. for the total energy $\frac{E_p - E_{gc}}{E_{gc}} 100\%$ where E_p and E_{gc} are the total energy measured in the proposed approach and GC respectively. Apart from E^+, all the metrics demonstrate statistical significance, i.e. $p < 0.05$ on a paired t-test. All but one participant showed

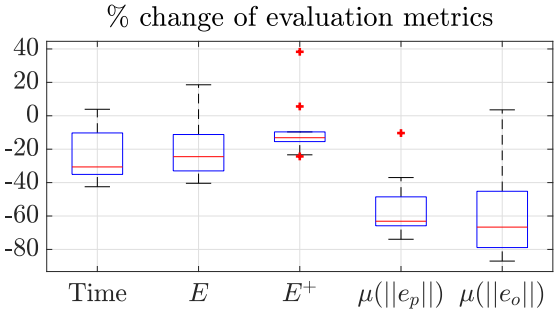

Fig. 4: Improvement achieved by the proposed controller wrt GC.

improved times, E and $\mu(||e_o||)$, while all participants had improved $\mu(||e_p||)$ with the proposed approach, and only two participants had increased the energy transferred from the user to the robot during their demonstration (E^+). In

particular, with our approach the total demonstration time was on average 24.6% lower compared to the GC with a median reduction of 30.6% among the subjects, while the total energy was on average 21% lower with a median reduction of 24.5%. The VF for guidance, enforcing the RTC, has improved the deviation from the surface and the normal angle, reducing the error on average by 55.3% and 55.8% respectively. Results indicate that the cognitive and physical load decreases, leading to increased efficiency and accuracy during demonstration. Notice in Fig.5 the elbow of the left robot arm being lower with the proposed method as compared to the GC to minimize the inertia metric. A typical time evolution of the inertia metric during demonstration is depicted in Fig.6, showing improvements for the duration of the demonstration. Similar results were observed for all other participants. Finally, throughout all the experiments, the joint limits were not violated due to the action of the joint limit avoidance signal.

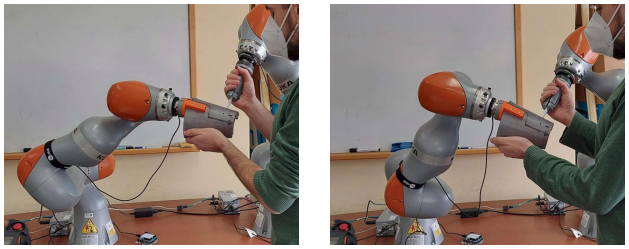

(a) [GC] **(b)** [Proposed]

Fig. 5: Snapshots of the experiment. The left elbow moves lower in the proposed approach decreasing the effective inertia.

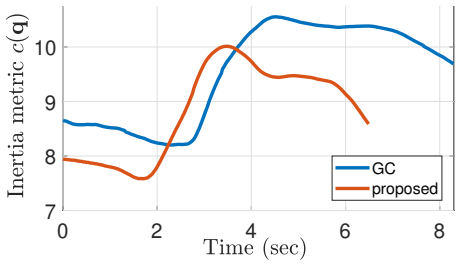

Fig. 6: Typical time evolution of the inertia metric.

V. Conclusions

In this work the problem of assisting the kinesthetic teaching of a bi-manual task with known workpiece geometry is addressed. The proposed control scheme combines the enforcement of task and joint limit VF as well as the null-space minimization of the effective inertia along the task DOFs. Experimental results with ten users show significant improvements in all the evaluation metrics as compared to the gravity compensation method. Future work includes further evaluation in challenging bi-manual tasks, like two-part assembly.

References

[1] H. Ravichandar, A. S. Polydoros, S. Chernova, and A. Billard, "Recent advances in robot learning from demonstration," *Annual Review of Control, Robotics, and Autonomous Systems*, vol. 3, no. 1, pp. 297–330, 2020.

[2] D. Vogt, S. Stepputtis, S. Grehl, B. Jung, and H. Ben Amor, "A system for learning continuous human-robot interactions from human-human demonstrations," in *2017 IEEE International Conference on Robotics and Automation (ICRA)*, pp. 2882–2889, 2017.

[3] P. Kormushev, D. N. Nenchev, S. Calinon, and D. G. Caldwell, "Upper-body kinesthetic teaching of a free-standing humanoid robot," in *2011 IEEE International Conference on Robotics and Automation*, pp. 3970–3975, 2011.

[4] D. Lee and C. Ott, "Incremental kinesthetic teaching of motion primitives using the motion refinement tube," *Autonomous Robots*, vol. 31, pp. 115–131, Oct 2011.

[5] D. Papageorgiou, F. Dimeas, T. Kastritsi, and Z. Doulgeri, "Kinesthetic guidance utilizing dmp synchronization and assistive virtual fixtures for progressive automation," *Robotica*, pp. 1–18.

[6] D. Papageorgiou and Z. Doulgeri, "A control scheme for haptic inspection and partial modification of kinematic behaviors*," in *2020 IEEE/RSJ International Conference on Intelligent Robots and Systems (IROS)*, pp. 9752–9758, 2020.

[7] D. Papageorgiou, S. Stavridis, C. Papakonstantinou, and Z. Doulgeri, "Task geometry aware assistance for kinesthetic teaching of redundant robots," in *2021 IEEE/RSJ International Conference on Intelligent Robots and Systems (IROS)*, pp. 7285–7291, 2021.

[8] N. Likar, B. Nemec, L. Žlajpah, S. Ando, and A. Ude, "Adaptation of bimanual assembly tasks using iterative learning framework," in *2015 IEEE-RAS 15th International Conference on Humanoid Robots (Humanoids)*, pp. 771–776, 2015.

[9] R. Lioutikov, O. Kroemer, G. J. Maeda, and J. Peters, "Learning manipulation by sequencing motor primitives with a two-armed robot," in *IAS*, 2014.

[10] È. Pairet, P. Ardón, M. N. Mistry, and Y. R. Pétillot, "Learning and composing primitive skills for dual-arm manipulation," in *TAROS*, 2019.

[11] L. P. Ureche and A. Billard, "Constraints extraction from asymmetrical bimanual tasks and their use in coordinated behavior," *Robotics and Autonomous Systems*, vol. 103, pp. 222–235, 2018.

[12] D. Papageorgiou, T. Kastritsi, Z. Doulgeri, and G. A. Rovithakis, "A passive phri controller for assisting the user in partially known tasks," *IEEE Transactions on Robotics*, vol. 36, no. 3, pp. 802–815, 2020.

[13] T. Kastritsi, D. Papageorgiou, I. Sarantopoulos, S. Stavridis, Z. Doulgeri, and G. A. Rovithakis, "Guaranteed active constraints enforcement on point cloud-approximated regions for surgical applications," in *2019 International Conference on Robotics and Automation (ICRA)*, pp. 8346–8352, 2019.

[14] S. A. Bowyer, B. L. Davies, and F. Rodriguez y Baena, "Active constraints/virtual fixtures: A survey," *IEEE Transactions on Robotics*, vol. 30, no. 1, pp. 138–157, 2014.

[15] M. Selvaggio, G. A. Fontanelli, F. Ficuciello, L. Villani, and B. Siciliano, "Passive virtual fixtures adaptation in minimally invasive robotic surgery," *IEEE Robotics and Automation Letters*, vol. 3, no. 4, pp. 3129–3136, 2018.

[16] H. Lin, K. Mills, P. Kazanzides, G. Hager, P. Marayong, A. Okamura, and R. Karam, "Portability and applicability of virtual fixtures across medical and manufacturing tasks," in *Proceedings 2006 IEEE International Conference on Robotics and Automation, 2006. ICRA 2006.*, pp. 225–230, 2006.

[17] F. Ficuciello, L. Villani, and B. Siciliano, "Variable impedance control of redundant manipulators for intuitive human–robot physical interaction," *IEEE Transactions on Robotics*, vol. 31, no. 4, pp. 850–863, 2015.

[18] J. G. Petersen and F. Rodriguez y Baena, "Mass and inertia optimization for natural motion in hands-on robotic surgery," in *2014 IEEE/RSJ International Conference on Intelligent Robots and Systems*, pp. 4284–4289, 2014.

[19] J. G. Petersen, S. A. Bowyer, and F. R. y. Baena, "Mass and friction optimization for natural motion in hands-on robotic surgery," *IEEE Transactions on Robotics*, vol. 32, no. 1, pp. 201–213, 2016.

[20] O. Khatib, "Inertial properties in robotic manipulation: An object-level framework," *The International Journal of Robotics Research*, vol. 14, no. 1, pp. 19–36, 1995.

[21] H.-J. Kang and R. Freeman, "Joint torque optimization of redundant manipulators via the null space damping method," in *Proceedings 1992 IEEE International Conference on Robotics and Automation*, pp. 520–525 vol.1, 1992.